ELSEVIER

Contents lists available at ScienceDirect

Journal of Luminescence

journal homepage: www.elsevier.com/locate/jlumin





Excitation dependent and time resolved photoluminescence of β -Ga₂O₃, β -(Ga_{0.955}Al_{0.045})₂O₃ and β -(Ga_{0.91}In_{0.09})₂O₃ epitaxial layers grown by pulsed laser deposition

Debabrata Das ^a, Francelia Sanchez Escobar ^{a,c}, Paul Gaurav Nalam ^{a,b}, Pallab Bhattacharya ^{d,**}, C.V. Ramana ^{a,b,*}

- ^a Centre for Advanced Materials Research (CMR), University of Texas at El Paso, 500 W University Ave, El Paso, TX, 79968, USA
- b Department of Mechanical Engineering, University of Texas at El Paso, 500 W University Ave, El Paso, TX, 79968, USA
- ^c Department of Metallurgical, Materials, and Biomedical Engineering, University of Texas at El Paso, 500 W University Ave, El Paso, TX, 79968, USA
- ^d Department of Electrical Engineering and Computer Science, University of Michigan, Ann Arbor, MI, 48109, USA

ARTICLE INFO

Keywords: β- Ga_2O_3 β- $(Ga_{0.95}Al_{0.045})_2O_3$ β- $(Ga_{0.91}In_{0.09})_2O_3$ Epitaxial thin fillm Pulsed laser deposition Photoluminescence spectroscopy

ABSTRACT

We have performed steady state and time-resolved photoluminescence measurements on β -Ga₂O₃ and β -(Ga_{0.955}Al_{0.045})₂O₃ and β -(Ga_{0.91}In_{0.09})₂O₃ mixed crystals grown by pulsed laser deposition. The steady state luminescence spectra of all the samples are characterized by transitions in the form of peaks and shoulders. In both Ga₂O₃ and the alloy oxides there are two transitions in the wavelength ranges of 330–381 nm (ultraviolet) and 486–492 nm (blue). Additionally, in Ga₂O₃, emissions at 596 nm (yellow) and 734 nm (near infrared) are also observed. Only the yellow transition is observed in (Ga_{0.955}Al_{0.045})₂O₃ at 582 nm and neither are observed in (Ga_{0.91}In_{0.09})₂O₃. Steady state and time-resolved photoluminescence measurements were also made as a function of excitation intensity. The trend of the variation of integrated and peak intensity, peak position and recombination lifetimes of the transitions with excitation are examined and discussed in the context of the underlying recombination mechanisms

1. Introduction

Monoclinic β -Ga₂O₃ is being investigated in recent years as an ultrawide bandgap semiconductor ($E_g^\sim 4.8$ eV) for application in high-power electronic devices [1–5]. It may even prove to be more suitable in this respect than GaN and SiC. At the same time, the large bandgap makes the oxide very promising for ultraviolet (UV) optoelectronics with applications such as UV solar blind photodetectors and scintillators, solar cells, and integrated chemical sensors [6–10]. Application of the oxides to light emitters is also important [11–13], which can provide the possibility of future optoelectronic integration with electronic devices. In this context, there are reports of luminescence studies on β -Ga₂O₃ [14–23] showing emission in the UV, blue, and red regions of the optical spectrum dependent on impurities and defects present in the material and some descriptions of the nature of the transitions leading to these emissions have been provided. Ga-Al-O and Ga-In-O are related oxide alloys, with bandgaps larger and smaller than that of Ga₂O₃, that will be

important in the design and ultimate realization of heterojunction light emitters. The alloys will also be useful for tuning the spectral response of photodetectors and solar cells and for the realization of quantum wells.

We have investigated photoluminescence spectra from unintentionally doped (UID) epitaxial $(Ga_{0.91}In_{0.09})_2O_3$ and $(Ga_{0.955}Al_{0.045})_2O_3$ and have compared them with those of Ga_2O_3 . While there exist several studies on undoped Ga_2O_3 , to the best of our knowledge, there is hardly any report on the photoluminescence behavior of $(Ga_{1-x}Al_x)_2O_3$ and $(Ga_{1-y}In_y)_2O_3$ ternary alloys. In the present study, excitation dependent photoluminescence (PL) and time-resolved PL (TRPL) measurements were made and the results have been analyzed in order to understand the underlying recombination mechanism of the transitions resulting in peaks and shoulders in the PL spectra.

E-mail addresses: pkb@umich.edu (P. Bhattacharya), rvchintalapalle@utep.edu (C.V. Ramana).

^{*} Corresponding author. Centre for Advanced Materials Research (CMR), University of Texas at El Paso, 500 W University Ave, El Paso, TX, 79968, USA.

^{**} Corresponding author.

2. Materials and methods

2.1. Target synthesis

Gallium oxide (Ga₂O₃) and Al/In mixed Ga₂O₃ pulsed laser deposition (PLD) targets were produced via the solid-state chemical reaction method [24]. In order to obtain the homogenous composites high purity Ga₂O₃ (99.999%) and Al₂O₃/In₂O₃ (99.999%) powders were mixed thoroughly. The ratio for Al/In was calibrated based on a stoichiometry following the chemical formula $Ga_2O_3/(Ga_{1-x}Al_x)_2O_3/(Ga_{1-v}In_v)_2O_3$, where x/y are the amounts of Al/In introduced. In the solid-state synthesis technique adopted, the process is initiated by grinding the powders using a mortar and pestle under a volatile liquid ambient. This confirms homogenous mixing and smaller size particle formation. The mixture was calcined at 1100 °C for 24 h in a muffle furnace. After calcination of the sample, the mixture was pulverized into a fine powder, which was then used to make ceramic pellets. The pellets had dimensions of 1 inch diameter and 1.5 mm thickness. The final stage of the PLD target synthesis involved sintering. The objective was to acquire a relatively concentrated material by eliminating the pores and defects that may have been present in the powder particles. The sintering temperature and duration were set at 1350 °C and 24 h, respectively.

2.2. Thin film deposition

 $Ga_2O_3/(Ga_{0.955}Al_{0.045})_2O_3/(Ga_{0.91}In_{0.09})_2O_3$ epitaxial films were deposited onto c-plane sapphire substrates. The background pressure in the growth chamber was 10^{-7} Torr before introducing oxygen. A KrF excimer laser with an output wavelength of 248 nm and with 230 mJ energy was used to ablate the target. Laser pulses with a 1-3 Hz pulse frequency were used to excite the ceramic target. The PLD target to substrate distance was maintained at 45 mm. The oxygen partial pressure in the growth chamber was held at 50 mTorr during deposition of the thin films. All the specifications were pre-optimized to obtain the best possible epitaxial film. The deposition of all the samples were made at a temperature of 700 $^{\circ}$ C. The controlled ablation of the PLD target generates a plasma plume containing micro and nano scale molecules and/or elemental Al/In/Ga/O atoms. The plasma particles, thus produced, are directed towards the sapphire substrate under a specific oxygen ambient for epitaxial film growth. The film thicknesses are determined from spectroscopic ellipsometer measurements and analysis of the measured data. Accordingly, the thicknesses of Ga₂O₃, $(Ga_{0.955}Al_{0.045})_2O_3$ and $(Ga_{0.91}In_{0.09})_2O_3$ are ~170 nm, 140 nm and 195 nm, respectively.

2.3. Characterization

X-ray diffraction (XRD) measurements were performed on all the samples using Rigaku Smartlab diffractometer in 1D mode with HyPix 3000 high energy resolution 2D HPAD detector. The Nano surf AFM system is used to give high resolution topography, deflection and phase contrast data. The optical absorption behavior of as grown samples is scrutinized through diffused reflectance spectroscopy. Jasco V-770 UV–Visible Spectrophotometer, with an optical resolution of 0.3 nm, has been employed to capture the spectrum. Photoluminescence measurements were made with a 80 MHz Ti: sapphire laser as the excitation source. 100 fs pulses at 245 nm were focused on the sample and the incident power density was varied in the range of 0.075–5.5 kW/cm². The luminescence was analyzed with a monochromator with a resolution of 0.02 mm and was detected with a photomultiplier tube. Transient signals in the TRPL measurements were detected by a high-speed single photon counter with a temporal resolution of 50 ps.

3. Results and discussion

XRD measurements performed on the Ga₂O₃ and alloyed thin films

indicate epitaxial film growth under optimum conditions. The data confirmed that all the epitaxial films are in the monoclinic phase with $(\overline{2}\ 01)$ orientation. The bandgap of $\beta\text{-}Ga_2O_3$ and the alloyed oxide semiconductors was derived from transmission measurements using a spectrophotometer with an optical resolution of 0.3 nm. The optical transmittance data (Fig. 1) indicate that all the samples are highly transparent. The recorded transmittance data were used to calculate the optical absorption of the samples. The band gap values derived are 4.81 eV, 4.94 eV, and 4.65 eV for Ga_2O_3 , $(Ga_{0.955}Al_{0.045})_2O_3$ and $(Ga_{0.91}In_{0.09})_2O_3$, respectively. The band gaps determined from optical absorption data confirm that Al-incorporation increases the band gap while alloying with In decreases the band gap.

Results obtained from steady state PL measurements are presented first. Fig. 2(a)-(c) show room-temperature PL spectra obtained from the Ga_2O_3 , $(Ga_{0.955}Al_{0.045})_2O_3$ and $(Ga_{0.91}In_{0.09})_2O_3$ samples. The spectra, with distinct peaks and shoulders, have been deconvolved with appropriate Gaussian functions to identify the various radiative transitions at different photon energies. The transition wavelengths in the three oxides are as follows. A transition in the ultraviolet (UV) region appears at 381 nm in Ga₂O₃. In the alloys this transition, shown in the insets, appears as a weak shoulder at 335 nm (3.7 eV) in $(Ga_{0.955}Al_{0.045})_2O_3$ and 330 nm (3.75 eV) in $(Ga_{0.91}In_{0.09})_2O_3$. The dominant peak in all three oxide appears in the blue region of the spectrum. The peak is at 486 nm in Ga_2O_3 and $(Ga_{0.955}Al_{0.045})_2O_3$ and at 492 nm in $(Ga_{0.91}In_{0.09})_2O_3$. Appearing as a weak shoulder is a transition in the yellow region of the spectrum, 596 nm in Ga_2O_3 and 582 in $(Ga_{0.955}Al_{0.045})_2O_3$. This transition is not clearly observed in (Ga_{0.91}In_{0.09})₂O₃. Also appearing as a visible shoulder in the spectrum of Ga₂O₃ is a transition in the red region at 734 nm (1.69 eV), which is not observed in the alloys. Measurements were made with the excitation on different spots on the surface and, in some cases, on multiple samples of the three oxide semiconductors. The general nature of the luminescence spectra of each was found to be consistent with those illustrated in Fig. 2 and described above. Excitation dependent PL measurements were also made with the excitation intensity varied over two orders of magnitude. The results are shown in Fig. 3(a)-(c). The incident power density was estimated from the laser power and spot size on the sample surface. It is evident that the intensity of all the peaks and shoulders increases with increasing excitation power. The increase of integrated PL intensity with incident power density for the dominant blue transitions in the three oxides and the UV transition (381 nm) in Ga₂O₃ is depicted in Fig. 4, together with the calculated slopes. These are the transitions for which reliable intensity values can be calculated. The corresponding plots exhibiting the dependence of peak PL intensity on excitation power are shown. Plots of the variation of the peak position of these two transitions (derived from the analyzed Gaussian fits) with incident power for the three oxides are

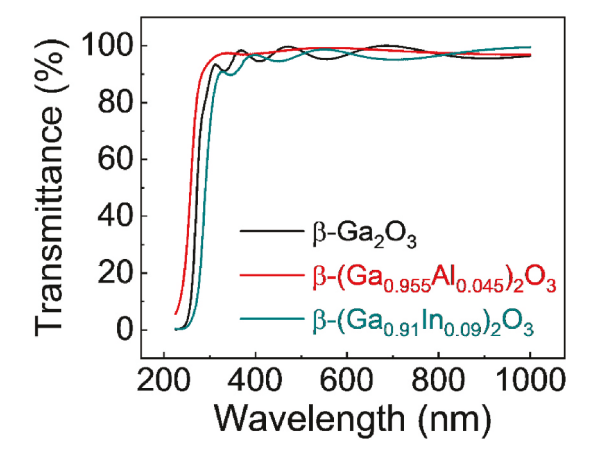


Fig. 1. Optical transmittance spectra of epitaxial β -Ga₂O₃, β -(Ga_{0.955}Al_{0.045})₂O₃ and β -(Ga_{0.91}In_{0.09})₂O₃ thin films.

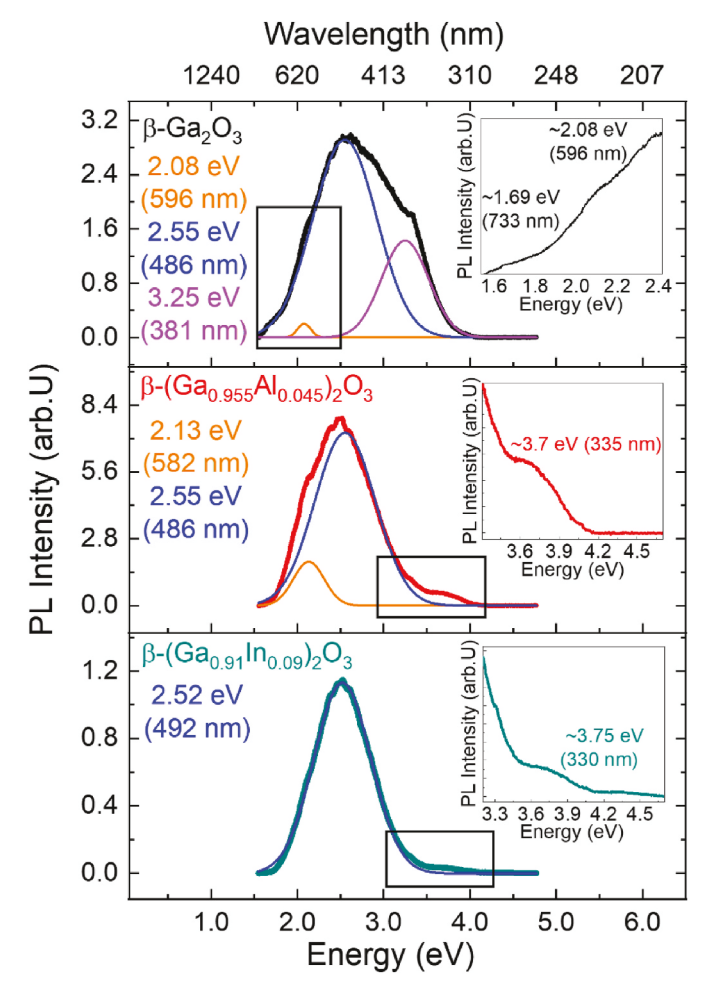


Fig. 2. Room temperature photoluminescence spectra of β -Ga₂O₃ (a), β -(Ga_{0.955}Al_{0.045})₂O₃ (b) and β -(Ga_{0.91}In_{0.09})₂O₃ (c) epitaxial layers. Inset in (c) shows magnified peak in UV region.

shown in Fig. 5. Except for a random spread in the data at very low incident powers, the peak positions of all the transitions in the three oxides are almost invariant with incident power, within limits of experimental error.

The excess carrier dynamics in the three oxides were investigated by transient PL measurements. These measurements were made at the UV and blue wavelengths in the PL spectra and with varying excitation power. Data obtained from the TRPL measurements at room temperature are shown in Fig. 6(a)-(c). The transient data were analyzed to yield

two time constants: an initial fast decay with a time constant τ_1 varying in the range of $\sim\!130\text{--}220$ ps followed by a slower decay with a time constant τ_2 varying in the range of $\sim\!0.9\text{--}1.9$ ns. Of the two time constants observed in the time-resolved PL decay of the various transitions, the shorter τ_1 is most likely associated with non-radiative recombination. The longer time constant τ_2 is in general agreement with the time constants $\sim\!2$ ns reported earlier from TRPL measurement on $\beta\text{--}Ga_2O_3^{23}$ and other wide bandgap materials such as GaN. It is also observed that there is no particular dependence of the time constants on excitation power density. The variation of τ_1 and τ_2 with excitation power for the three transitions in $(Ga_{0.955}\text{Al}_{0.045})_2O_3$ is depicted in Fig. 7.

In elucidating the nature of the various transitions in the three oxides, it is worthwhile to note the following. The exciton binding energy in Ga₂O₃ is over 100 meV, with reported values [25-27] in the range 120-270 meV. Excitonic photoresponse has been measured at room temperature in Ga_2O_3/GaN photodetectors [28]. The exciton can bind to defects and impurities in the materials and from bound excitons, that can also exist at room temperature. It is also known that self-trapped excitons (STEs) are very stable in Ga₂O₃ [29], and is expected to exhibit the same behavior in $(Ga_{0.955}Al_{0.045})_2O_3$ and $(Ga_{0.91}In_{0.09})_2O_3$. Exciton-related luminescence transitions generally exhibit invariant spectral peak position and recombination lifetime with variation of excitation power. We have recently confirmed these trends in monolayer GaN with an exciton binding energy of 95 meV [30]. In addition, it has generally been observed experimentally [31] that the dependence of PL intensity I_{PL} on excitation power I_{exc} can be expressed as $I_{PL} \propto I_{exc}^k$, where the exponent k ranges between 1 and 2 for free- and bound-exciton transitions and k < 1 for free-to-bound (FB) and donor-acceptor (DA) pair transitions [30–32].

The UV emission observed in Ga₂O₃ in Fig. 2(a) is also present in the spectra of (Ga_{0.955}Al_{0.045})₂O₃ (Fig. 2(b)) and (Ga_{0.91}In_{0.09})₂O₃ (Fig. 2 (c)). This emission is intrinsic in the oxides and is a result of the recombination of free electrons with self-trapped holes (STH) [15,22, 33-36], or the recombination of self-trapped electrons (STE) [16,22,29, 37]. Our excitation-dependent intensity, recombination lifetime and spectral peak position data support this. The emission in the blue region is dominant in Ga₂O₃ (486 nm) and is dominant in (Ga_{0.955}Al_{0.045})₂O₃ (486 nm) and (Ga_{0.91}In_{0.09})₂O₃ (492 nm) also. It is also believed to be intrinsic in Ga₂O₃ and has been attributed to a DA transition involving native defects V_{O} (donors) and V_{Ga} or $V_{Ga}\mbox{-}V_{O}$ complexes (acceptors) [14-17,22,23]. Our excitation dependent PL data of intensity (k~1), peak position and recombination lifetime strongly suggest the involvement of excitons in this transition. With a binding energy larger than 100 meV, excitons are not dissociated at room temperature. Even with exciton binding energies ~20-30 meV, there are light modulators and light sources based on excitonic phenomena operating at room temperature. In wide band semiconductors the impurity levels, and particularly the acceptors, form bands near the band edge [23,38]. For DA and

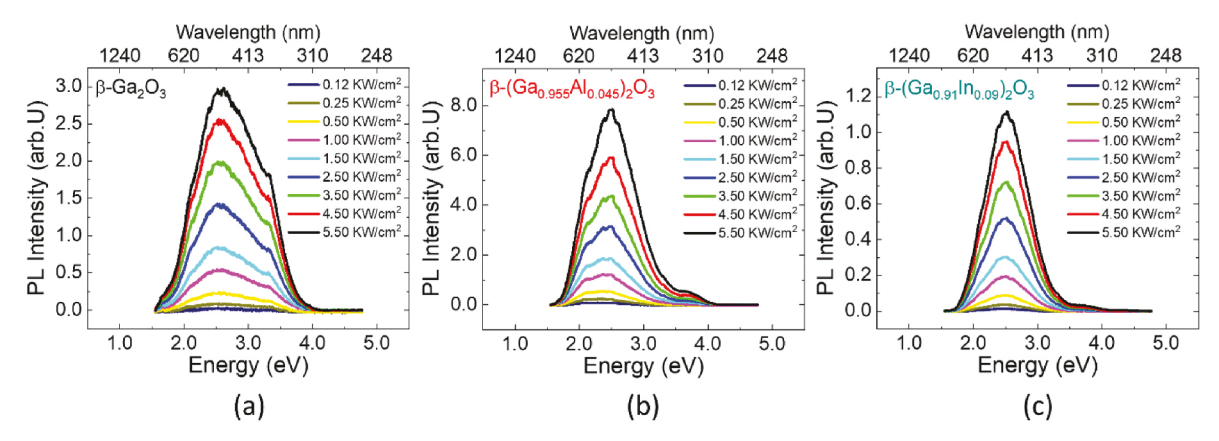


Fig. 3. Room temperature excitation dependent photoluminescence response of β-Ga₂O₃ (a), β-(Ga_{0.955}Al_{0.045})₂O₃ (b) and β-(Ga_{0.91}In_{0.09})₂O₃ (c) thin films.

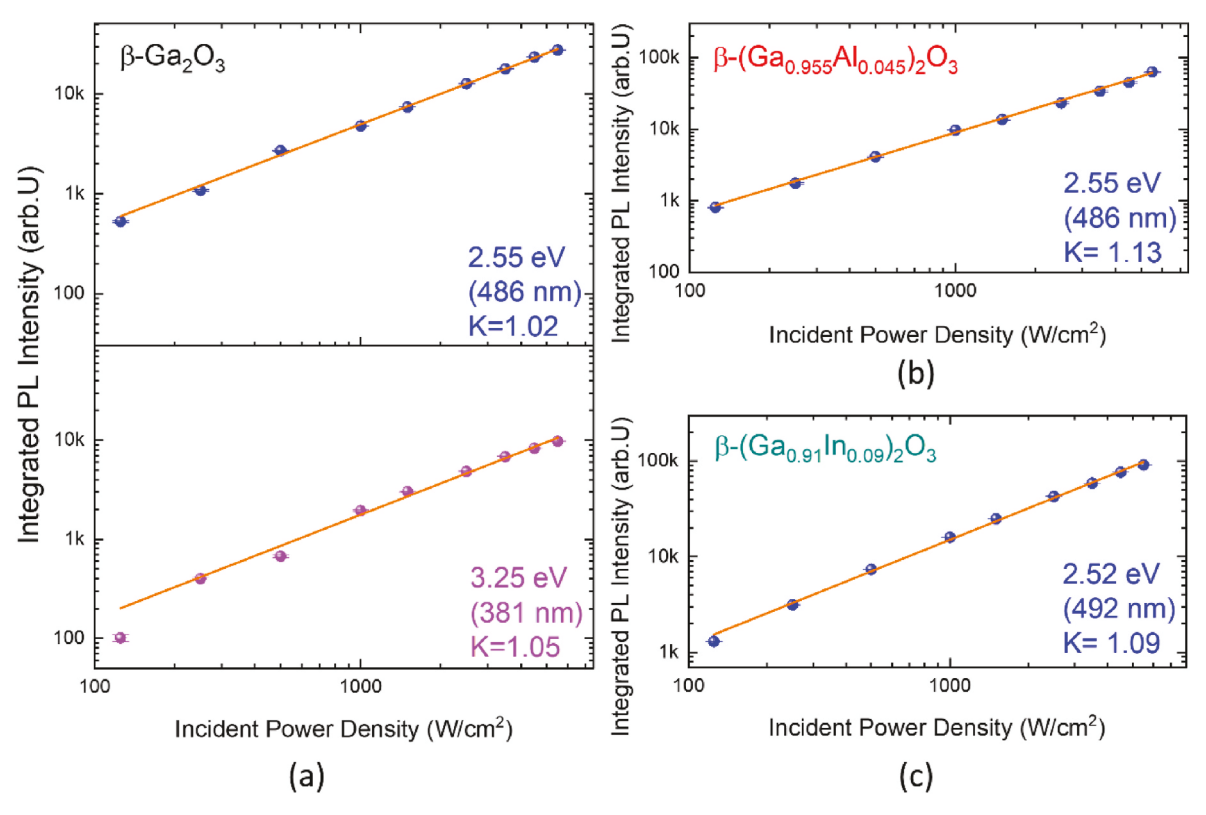
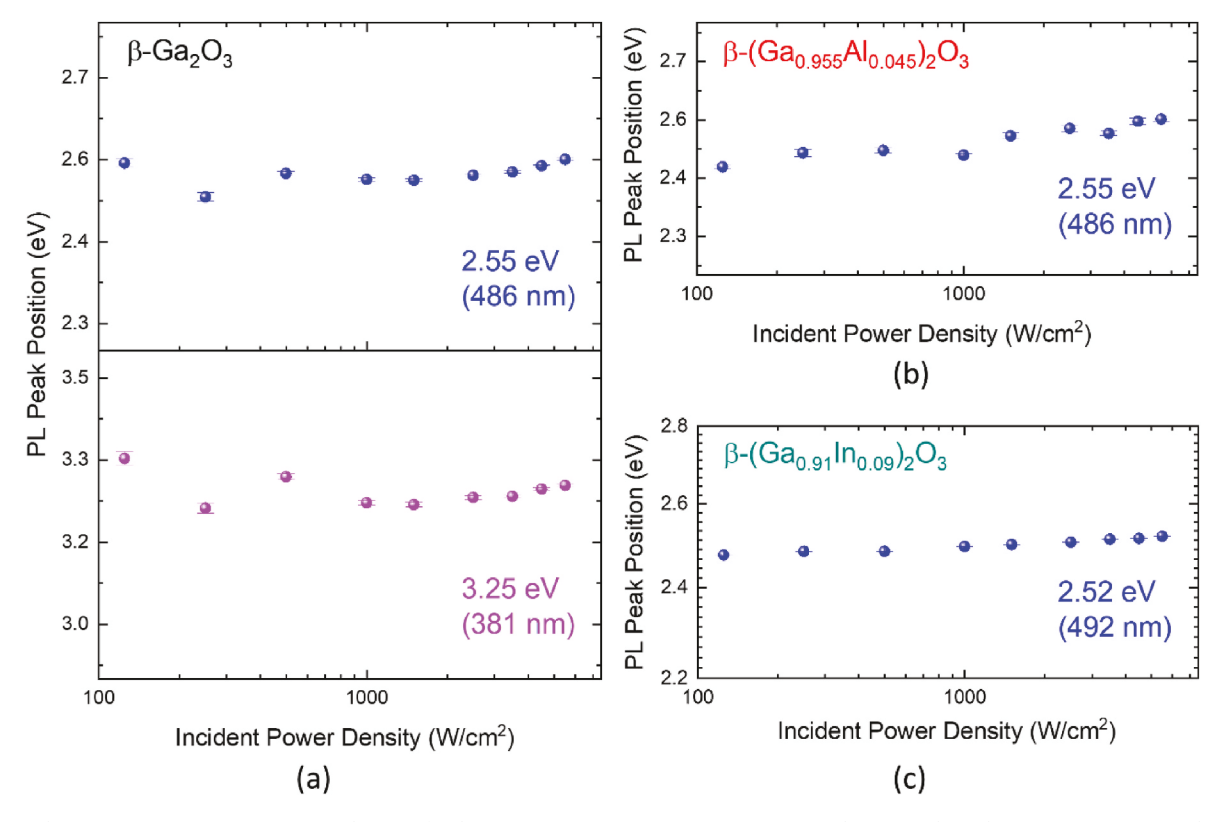


Fig. 4. Plots of integrated photoluminescence intensity versus excitation power density of blue and UV transitions in β-Ga₂O₃ (a), β-(Ga_{0.955}Al_{0.045})₂O₃ (b) and β-(Ga_{0.91}In_{0.09})₂O₃ (c) thin films.



 $\textbf{Fig. 5.} \ \ \text{Peak position versus excitation power density of radiative transitions in } \beta\text{-}Ga_2O_3 \ (a), \ \beta\text{-}(Ga_{0.955}Al_{0.045})_2O_3 \ (b) \ \ \text{and} \ \beta\text{-}(Ga_{0.91}In_{0.09})_2O_3 \ (c) \ \ \text{thin films.}$

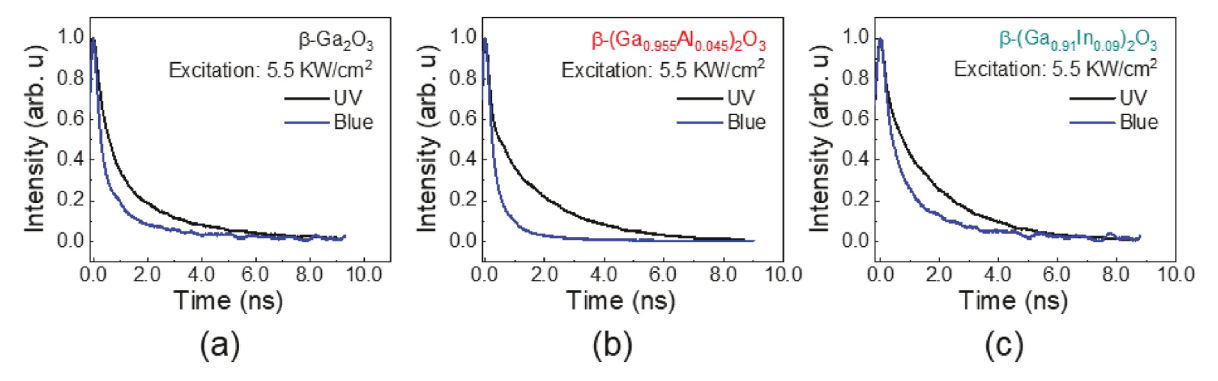


Fig. 6. Transient photoluminescence response in β-($Ga_{0.955}Al_{0.045}$)₂O₃ thin films.

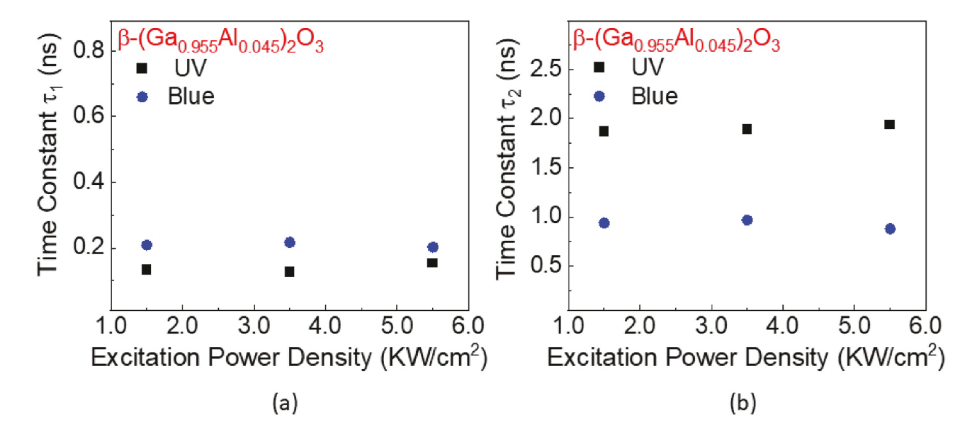


Fig. 7. Variation of photoluminescence decay time constants τ_1 and τ_2 with excitation power density in β -(Ga_{0.955}Al_{0.045})₂O₃.

FB transitions in this case the peak position would shift and the linewidth would change due to state filling effects. These trends are not observed here. Therefore we suggest, with caution, that the dominant transition in the blue region may involve the recombination of excitons bound to native defects or the recombination of STEs formed with the involvement of native defects. Further investigations are needed for confirmation. There are two more transitions, that appear as weak shoulders in the PL spectrum of Ga₂O₃ in Fig. 2(a). These transitions at 1.69 eV (734 nm) and 2.08 eV (596 nm) are highlighted in the inset of the figure. Only a shoulder is observed at 2.13 eV (582 nm) in the spectrum of $(Ga_{0.955}Al_{0.045})_2O_3$ (Fig. 2(b)) and none are observed in the spectrum of $(Ga_{0.91}In_{0.09})_2O_3$ (Fig. 2(c)). Transitions at \sim 590 nm (yellow) that are observed here and 520 nm (green, not detected in the oxides investigated in this study) have been reported in undoped and Zn-doped Ga₂O₃ [13,37] and they possibly result from a DA recombination between $V_{\rm O}$ (donors) and $V_{\rm Ga}\text{-}V_{\rm O}$ (acceptors). In the case of UID Ga₂O₃ and (Ga_{0.955}Al_{0.045})₂O₃ investigated here, it is also possible that the transitions at 596 and 582 nm, respectively, result from ubiquitous impurities present in small amounts. The transition appearing as a shoulder in the spectrum of Ga₂O₃ at 1.69 eV (734 nm) in Fig. 2(a) is not observed in the spectra of $(Ga_{0.955}Al_{0.045})_2O_3$ and $(Ga_{0.91}In_{0.09})_2O_3$. Transitions in the red to near-infrared spectral region, ranging from 620 to 720 nm have been observed in UID and intentionally doped Ga₂O₃. These longer wavelength transitions have ben related to Fe [19,22] and Cr [17,22,39,40], in particular, and also to N [22] and rare-earth elements Eu and Er [13]. Cr³⁺ ions are present as an uncontrolled impurity and N can be unintentionally incorporated during PLD target preparation. However, from the present study it appears that alloying Ga₂O₃ with Al or In eliminates the red recombination transition, or makes it too weak to be observed in the PL spectra. The transitions in the red spectral region have been attributed to DA recombination [23], where the donor and acceptor species may vary depending on unintentional or intentional impurities present. It is interesting to note that transitions in the red region are absent, or below the detections limit, in the alloys. The reason is not understood at this time.

4. Conclusions

In conclusion, we have investigated the spontaneous emission characteristics of UID epitaxial $(Ga_{0.955}Al_{0.045})_2O_3$ and $(Ga_{0.91}In_{0.09})_2O_3$ layers with excitation dependent steady-state and time-resolved photoluminescence measurements and have compared them with the emission characteristics of epitaxial UID Ga_2O_3 . The epitaxial layers were grown on sapphire substrates with precisely controlled seed layers. Dominant transitions in the UV and blue regions of the spectrum are observed in the PL spectra of Ga_2O_3 and both alloy oxides. In contrast, transitions in the red to infrared and yellow regions of the spectrum, that have been associated with trace unintentional impurities, are seen as very weak shoulders in the spectrum of Ga_2O_3 , but are absent in the alloy oxides. The nature of the recombination mechanism of the different transitions are discussed.

Author contributions and statement

CVR and PB conceived and supervised the research. DD, PGN, and FS synthesized samples. DD and FS collected the structural data. All authors were involved in data analyses, designed figures, and wrote the manuscript. PB and DD coordinated to collect the comments and feedback from all co-authors. Finally, all the authors approved the submission.

Data availability statement

The scientific data and analyses are included in the manuscript. The other data that do not appear in the manuscript may be available by a

reasonable request from the corresponding author.

Declaration of competing interest

The authors declare that they have no known competing financial interests or personal relationships that could have appeared to influence the work reported in this paper.

Acknowledgements

This material is based upon work supported by the Air Force Office of Scientific Research (AFOSR) under award number FA9550-21-1-0360. However, any opinions, findings, and conclusions or recommendations expressed in this material are those of the author(s) and do not necessarily reflect the views of the United States Air Force. The authors at the University of Texas at El Paso also acknowledge, with pleasure, support from the National Science Foundation (NSF) with NSF-PREM grant #DMR-1827745. The work at the University of Michigan was supported by the College of Engineering under the Blue Sky Research Program.

References

- [1] J. Kim, M.A. Mastro, M.J. Tadjer, J. Kim, Heterostructure WSe₂-Ga₂O₃ junction field-effect transistor for low-dimensional high-power electronics, ACS Appl. Mater. Interfaces 10 (35) (2018) 29724–29729.
- [2] M. Higashiwaki, K. Sasaki, A. Kuramata, T. Masui, S. Yamakoshi, Gallium oxide (Ga_2O_3) metal-semiconductor field-effect transistors on single-crystal β -Ga $_2O_3$ (010) substrates, Appl. Phys. Lett. 100 (1) (2012), 013504.
- [3] H. Zhou, K. Maize, J. Noh, A. Shakouri, P.D. Ye, Thermodynamic studies of β-Ga₂O₃ nanomembrane field-effect transistors on a sapphire substrate, ACS Omega 2 (11) (2017) 7723–7729.
- [4] K. Tetzner, E.B. Treidel, O. Hilt, A. Popp, S.B. Anooz, G. Wagner, A. Thies, K. Ickert, H. Gargouri, J. Würfl, Lateral 1.8 kV β-Ga₂O₃ MOSFET with 155 MW/cm² power figure of merit, IEEE Electron. Device Lett. 40 (9) (2019) 1503–1506.
- [5] M.H. Wong, H. Murakami, Y. Kumagai, M. Higashiwaki, Enhancement-mode β-Ga₂O₃ current aperture vertical MOSFETs with N-Ion-Implanted blocker, IEEE Electron. Device Lett. 41 (2) (2020) 296–299.
- [6] H. Liang, S. Cui, R. Su, P. Guan, Y. He, L. Yang, L. Chen, Y. Zhang, Z. Mei, X. Du, Flexible X-ray detectors based on amorphous Ga₂O₃ thin films, ACS Photonics 6 (2) (2018) 351–359
- [7] H. Dong, S. Pang, Y. Xu, Z. Li, Z. Zhang, W. Zhu, D. Chen, H. Xi, Z. Lin, J. Zhang, Y. Hao, C. Zhang, Ultrawide band gap oxide semiconductor-triggered performance improvement of perovskite solar cells via the novel Ga₂O₃/SnO₂ composite electron-transporting bilayer, ACS Appl. Mater. Interfaces 12 (49) (2020) 54703–54710.
- [8] K. Arora, N. Goel, M. Kumar, M. Kumar, Ultrahigh performance of self-powered β -Ga₂O₃ thin film solar-blind photodetector grown on cost-effective Si substrate using high-temperature seed layer, ACS Photonics 5 (6) (2018) 2391–2401.
- [9] S.J. Pearton, J. Yang, P.H. Cary, F. Ren, J. Kim, M.J. Tadjer, M.A. Mastro, A review of Ga₂O₃ materials, processing, and devices, Appl. Phys. Rev. 5 (1) (2018), 011301.
- [10] A.S. Pratiyush, S. Krishnamoorthy, S.V. Solanke, Z. Xia, R. Muralidharan, S. Rajan, D.N. Nath, High responsivity in molecular beam epitaxy grown β-Ga₂O₃ metal semiconductor metal solar blind deep-UV photodetector, Appl. Phys. Lett. 110 (22) (2017) 221107.
- [11] C.-H. Lin, C.-T. Lee, Ga₂O₃-based solar-blind deep ultraviolet light-emitting diodes, J. Lumin. 224 (2020) 117326.
- [12] H. Wang, G. Xiang, Y. Zhou, W. Peng, Y. Liu, J. Zhang, J. Zhang, R. Li, Y. Zhao, Excellent electroluminescence and electrical characteristics from p-CuO/i-Ga₂O₃/ n-GaN light-emitting diode prepared by magnetron sputtering, J. Lumin. 243 (2022) 118621.
- [13] G. Deng, Y. Huang, Z. Chen, C. Pan, K. Saito, T. Tanaka, Q. Guo, Yellow emission from vertically integrated Ga_2O_3 doped with Er and Eu electroluminescent film, J. Lumin. 235 (2021) 118051.
- [14] L. Binet, D. Gourier, Origin of the blue luminescence of β-Ga₂O₃, J. Phys. Chem. Solid. 59 (8) (1998) 1241–1249.
- [15] T. Onuma, S. Fujioka, T. Yamaguchi, M. Higashiwaki, K. Sasaki, T. Masui, T. Honda, Correlation between blue luminescence intensity and resistivity in β-Ga₂O₃ single crystals, Appl. Phys. Lett. 103 (4) (2013), 041910.
- [16] T. Onuma, Y. Nakata, K. Sasaki, T. Masui, T. Yamaguchi, T. Honda, A. Kuramata, S. Yamakoshi, M. Higashiwaki, Modeling and interpretation of UV and blue

- luminescence intensity in β -Ga₂O₃ by silicon and nitrogen doping, J. Appl. Phys. 124 (7) (2018), 075103.
- [17] A. Luchechko, V. Vasyltsiv, L. Kostyk, O. Tsvetkova, A.I. Popov, Shallow and deep trap levels in X-ray irradiated β -Ga₂O₃: Mg, Nucl. Instrum. Methods Phys. Res. B 441 (2019) 12–17.
- [18] N. Makeswaran, D. Das, V. Zade, P. Gaurav, V. Shutthanandan, S. Tan, C. V. Ramana, Size-and phase-controlled nanometer-thick β-Ga₂O₃ films with green photoluminescence for optoelectronic applications, ACS Appl. Nano Mater. 4 (4) (2021) 3331–3338.
- [19] R. Sun, Y.K. Ooi, P.T. Dickens, K.G. Lynn, M.A. Scarpulla, On the origin of red luminescence from iron-doped β-Ga₂O₃ bulk crystals, Appl. Phys. Lett. 117 (5) (2020), 052101.
- [20] W. Mi, J. Ma, C. Luan, H. Xiao, Structural and optical properties of β -Ga₂O₃ films deposited on MgAl₂O₄ (1 0 0) substrates by metal–organic chemical vapor deposition, J. Lumin. 146 (2014) 1–5.
- [21] T. Zhang, J. Lin, X. Zhang, Y. Huang, X. Xu, Y. Xue, J. Zou, C. Tang, Single-crystalline spherical β-Ga₂O₃ particles: synthesis, N-doping and photoluminescence properties, J. Lumin. 140 (2013) 30–37.
- [22] G. Naresh-Kumar, H. MacIntyre, S. Subashchandran, P.R. Edwards, R.W. Martin, K. Daivasigamani, K. Sasaki, A. Kuramata, Origin of red emission in β-Ga₂O₃ analyzed by cathodoluminescence and photoluminescence spectroscopy, Phys. Status Solidi B 258 (2) (2021) 2000465.
- [23] K.M. Othonos, M. Zervos, C. Christofides, A. Othonos, Ultrafast spectroscopy and red emission from β-Ga₂O₃/β-Ga₂S₃ nanowires, Nanoscale Res. Lett. 10 (1) (2015) 1016.
- [24] G. Gutierrez, E.M. Sundin, P.G. Nalam, V. Zade, R. Romero, A.N. Nair, S. Sreenivasan, D. Das, C. Li, C.V. Ramana, Interfacial phase modulation-induced structural distortion, band gap reduction, and nonlinear optical activity in tinincorporated Ga₂O₃, J. Phys. Chem. C 37 (2021) 20468–20481.
- [25] A. Mock, R. Korlacki, C. Briley, V. Darakchieva, B. Monemar, Y. Kumagai, K. Goto, M. Higashiwaki, M. Schubert, Band-to-band transitions, selection rules, effective mass, and excitonic contributions in monoclinic β–Ga₂O₃, Phys. Rev. B 96 (24) (2017) 245205.
- [26] F. Bechstedt, J. Furthmüller, Influence of screening dynamics on excitons in Ga₂O₃ polymorphs, Appl. Phys. Lett. 114 (12) (2019) 122101.
- [27] C. Sturm, R. Schmidt-Grund, V. Zviagin, M. Grundmann, Temperature dependence of the dielectric tensor of monoclinic Ga₂O₃ single crystals in the spectral range 1.0–8.5 eV, Appl. Phys. Lett. 111 (8) (2017), 082102.
- [28] R. Tang, G. Li, Y. Jiang, N. Gao, J. Li, C. Li, K. Huang, J. Kang, T. Wang, R. Zhang, Ga₂O₃/GaN heterostructural ultraviolet photodetectors with exciton-dominated ultranarrow response, ACS Appl. Electron. Mater. 4 (1) (2021) 188–196.
- [29] S. Yamaoka, M. Nakayama, Evidence for formation of self-trapped excitons in a β-Ga₂O₃ single crystal, Phys. Status Solidi C 13 (2–3) (2016) 93–96.
- [30] A. Aiello, Y. Wu, A. Pandey, P. Wang, W. Lee, D. Bayerl, N. Sanders, Z. Deng, J. Gim, K. Sun, R. Hovden, E. Kioupakis, Z. Mi, P. Bhattacharya, Deep ultraviolet luminescence due to extreme confinement in monolayer GaN/Al(Ga)N nanowire and planar heterostructures, Nano Lett. 19 (11) (2019) 7852–7858.
- [31] T. Schmidt, K. Lischka, W. Zulehner, Excitation-power dependence of the near-band-edge photoluminescence of semiconductors, Phys. Rev. B 45 (16) (1992) 8989–8994.
- [32] Y. Hwang, Y. Um, H. Park, Temperature and excitation power dependences of the photoluminescence in CdMnTe crystals, J. Kor. Phys. Soc. 58 (51) (2011) 1312–1315
- [33] J.B. Varley, A. Janotti, C. Franchini, C.G. Van de Walle, Role of self-trapping in luminescence and p-type conductivity of wide-band-gap oxides, Phys. Rev. B 85 (8) (2012), 081109.
- [34] A. Kyrtsos, M. Matsubara, E. Bellotti, On the feasibility of p-type Ga₂O₃, Appl. Phys. Lett. 112 (3) (2018), 032108.
- [35] T. Gake, Y. Kumagai, F. Oba, First-principles study of self-trapped holes and acceptor impurities in Ga₂O₃ polymorphs, Phys. Rev. Mater. 3 (4) (2019), 044603.
- [36] M.D. McCluskey, Point defects in Ga₂O₃, J. Appl. Phys. 127 (10) (2020) 101101.
- [37] J. Jiang, J. Zhang, Z. Song, Influence of Zn doping on the morphology and luminescence of Ga₂O₃ low-dimensional nanostructures, J. Lumin. 221 (2020) 117048.
- [38] A. Pandey, X. Liu, Z. Deng, W.J. Shin, D.A. Laleyan, K. Mashooq, E.T. Reid, E. Kioupakis, P. Bhattacharya, Z. Mi, Enhanced doping efficiency of ultrawide band gap semiconductors by metal-semiconductor junction assisted epitaxy, Phys. Rev. Mater. 3 (5) (2019), 053401.
- [39] A. Luchechko, V. Vasyltsiv, Y. Zhydachevskyy, M. Kushlyk, S. Ubizskii, A. Suchocki, Luminescence spectroscopy of Cr^{3+} ions in bulk single crystalline β -Ga₂O₃, J. Phys. D Appl. Phys. 53 (35) (2020) 354001.
- [40] A. Luchechko, V. Vasyltsiv, L. Kostyk, O. Tsvetkova, B. Pavlyk, The effect of Cr^{3+} and Mg^{2+} impurities on thermoluminescence and deep traps in β -Ga₂O₃ crystals, ECS J. Solid State Sci. Technol. 9 (4) (2020), 045008.